ISSN 1054-660X, Laser Physics, 2011, Vol. 21, No. 8, pp. 1518–1524.

Generation of Long Broadband Pulses with a Figure-Eight Fiber Laser[1]

J. C. Hernandez-Garcia[a, *], O. Pottiez[a], R. Grajales-Coutiño[b], B. Ibarra-Escamilla[c], E. A. Kuzin[c], J. M. Estudillo-Ayala[d], and J. Gutierrez-Gutierrez[b]

[a] *Centro de Investigaciones en Optica (CIO), Loma del Bosque 115, Col. Lomas del Campestre, Leon, Gto. 37150, Mexico*

[b] *Escuela de Ciencias, Universidad Autonoma "Benito Juarez" de Oaxaca, Av. Universidad s/n, Oaxaca, Oax. 68120, Mexico*

[c] *Instituto Nacional de Astrqfisica, Optica y Electronica (INAOE), Departamento de Optica, L. E. Erro 1, Puebla, Pue. 72000, Mexico*

[d] *Division de Ingenierias Campus Irapuato-Salamanca, Universidad de Guanajuato, Carretera Salamanca-Valle de Santiago Km 3.5+1.8 Km, Comunidad de Palo Blanco, Salamanca, Gto., 36885, Mexico*

*e-mail: juancarlos@cio.mx

Received September 28, 2010; in final form November 11, 2010; published online July 4, 2011

Abstract—In this paper we performed the experimental and numerical study of a passively mode-locked fiber laser that generates packets of sub-picosecond pulses instead of individual pulses. The proposed configuration is a figure-eight fiber laser scheme, which includes a Nonlinear Optical Loop Mirror with polarization asymmetry inserted into a ring cavity. No experimental evidence of self-starting mode locking operation of the laser was observed; however, for proper adjustments of the wave retarders included in the setup, a mechanical stimulation triggers the onset of mode locking. The autocorrelation of the generated pulses shows a narrow sub-picosecond peak riding a large sub-nanosecond pedestal whose intensity is half that of the peak, and the optical spectrum is smooth and wide. We show that contrary to conventional ultrashort pulses, these pulses do not vanish rapidly after propagation through a long dispersive fiber, which makes then attractive for supercontinuum generation as well as for applications in metrology. Finally, we study the pulse formation in the laser and present arguments based on experimental data and numerical simulations that the observed pulses are actually sets of a large number of solitons.

DOI: 10.1134/S1054660X11150114

INTRODUCTION

Passively mode-locked fiber lasers are simple, compact and low-cost sources of sub-picosecond optical pulses. Among the existing schemes, the fiber ring laser has attracted considerable attention due to its simple design and compactness [1, 2]. In recent works, this scheme was implemented to allow the generation of giant-chirped pulses in the large normal dispersion regime [3], to demonstrate wide range wavelength tuning of the pulse train by using graphene as the saturable absorber [4], or for the generation of dual-wavelength solitons [5], among other applications. Another attractive architecture is the figure-eight laser [6, 7], where the saturable absorber action is provided by the nonlinear transmission characteristic of a Nonlinear Optical Loop Mirror (NOLM) [8], or alternatively of a Nonlinear Amplifying Loop Mirror (NALM) [9] or of a NOLM including a semiconductor optical amplifier (SOA), which is more compact although larger pulse durations are obtained due to the slow dynamics of the semiconductor element [10]. Let us mention finally the linear cavity architecture, in particular incorporating a semiconductor saturable absorber mirror (SESAM) for mode locking, which allowed recently the generation of high-energy pulses at ultra-low repetition rate from a very long cavity [11].

Although in most NOLM architectures, switching relies on a power imbalance between the beams that counter-propagate in the loop, an attractive design based on polarization asymmetry was also proposed [12]. The device is power-symmetric, as a 50/50 coupler is used, and polarization symmetry is broken by a quarter wave retarder (QWR) inserted in the loop. Due to the QWR, the counter-propagating beams have different polarizations and accumulate different amounts of nonlinear polarization rotation (NPR), which allows switching. The device advantages, in particular in the frame of figure-eight lasers, include its robustness and the flexibility of its nonlinear switching characteristic, which can be adjusted through the orientation of the QWR or the choice of input polarization. Stable sub-ps pulse generation [13] and self-starting mode locking operation [14] were demonstrated using this scheme. Moreover, if the angle of linear polarization is controlled at the NOLM input, the switching

[1] The article is published in the original.

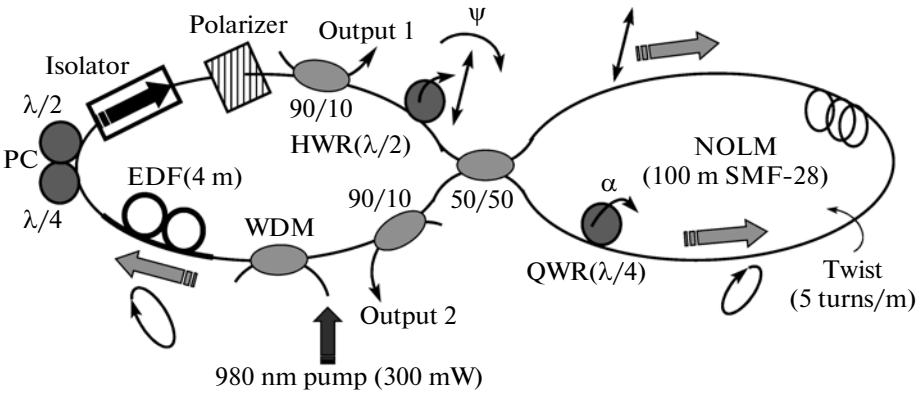

Fig. 1. Scheme of the figure-eight laser under study.

power can be chosen adequately to obtain more easily the mode locking operation [15].

The generation of ultrashort optical pulses is useful for many applications. For some of them, like supercontinuum generation [16, 17], development of multiwavelength lasers [5, 18] or metrology [19], desirable characteristics include high pulse energy, large optical bandwidth and low temporal coherence. A typical drawback of fiber sources used for ultrashort pulse generation is the relatively low energy of the pulses, which translates into low average output powers. The limitation in pulse energy and peak power is imposed by the strong nonlinearities in the fiber, where light is tightly confined into the core and where the nonlinear phase shift accumulates over long distances, ultimately provoking pulse breaking. In anomalous dispersion soliton fiber lasers, where pulse formation results from a balance between Kerr nonlinearity and anomalous dispersion, pulse energy is limited to ~0.1 nJ [20]. By using dispersion management to reduce effective peak power, this limit was increased to 2–3 nJ with the so-called stretched-pulse fiber lasers [21, 22]. Pulse energies higher than 10 nJ were recently obtained from a mode-locked fiber laser in the anomalous-dispersion regime, however the use of large mode-area photonic crystal fiber was required [23]. In [11], pulses with energies as high as 75 nJ were generated from a long linear cavity including a SESAM, however their bandwidth was not higher than a few nanometers. Moreover, in the linear regime, when ultrashort pulses propagate through a long dispersive fiber, they broaden temporally and their peak power rapidly vanishes. This reduces the interest of these pulses for some applications in metrology, in particular measurements that need to be earned out through long segments of fiber.

In this paper, we propose and study a passively mode-locked figure-eight fiber laser that generates sub-nanosecond wave packets with sub-picosecond temporal coherence, > nanojoules energy and a wide bandwidth of several tens of nm. Finally, the experimental results are confirmed by numerical simulations.

1. EXPERIMENTAL SETUP

The figure-eight laser is formed, as shown in Fig. 1, by a NOLM (on the right side) inserted in a ring laser cavity (left part). The NOLM includes a symmetric coupler, which ensures a power-symmetric operation. The output ports of the coupler were fusion-spliced with a 100 m loop of low-birefringence SMF-28 fiber. The fiber loop has an anomalous dispersion of ~17 ps (nm km)$^{-1}$ and a nonlinear coefficient γ = 1.5 (W km)$^{-1}$ for linearly polarized light. A QWR plate is inserted in the loop, this device transforms the polarization of the counter-clockwise beam from linear to elliptic, the value of ellipticity depending on the relative angle ψ between the QWR and the polarizer in the ring section. A twist rate of 5 turns/m is imposed to the fiber loop, which is used to eliminate residual fiber birefringence so that the fiber behaves like an ideal isotropic fiber [24]. The operation of the NOLM is based on NPR, and allows great flexibility of the device transmission characteristic, which can be adjusted through the orientation of the angles α and ψ (shown in Fig. 1).

One important aspect of the experimental setup is that the polarization state at the NOLM input is linear, and its angle ψ defined with respect to the QWR axes can be adjusted. The adjustment of the angle ψ allows adjusting the NOLM switching power. The expression that determines switching power is given by

$$P_{\pi\psi} = \frac{4\pi}{\beta L \sin(2\psi)}, \quad (1)$$

where L is the length of the NOLM loop, β is the nonlinear coefficient for circular polarization associated with the nonlinear coefficient for linear polarization γ by

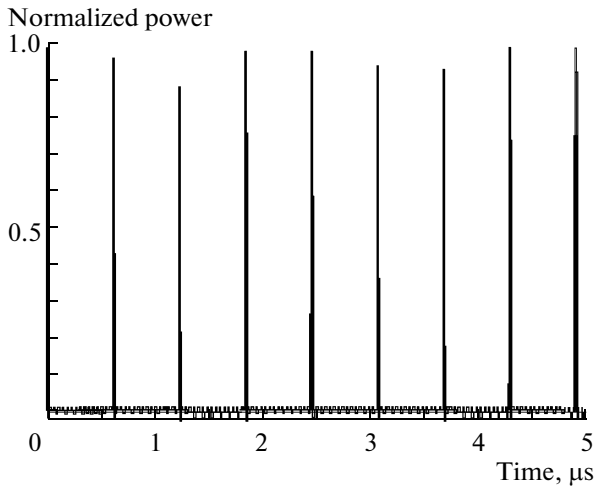

Fig. 2. Oscilloscope trace of the optical pulse train.

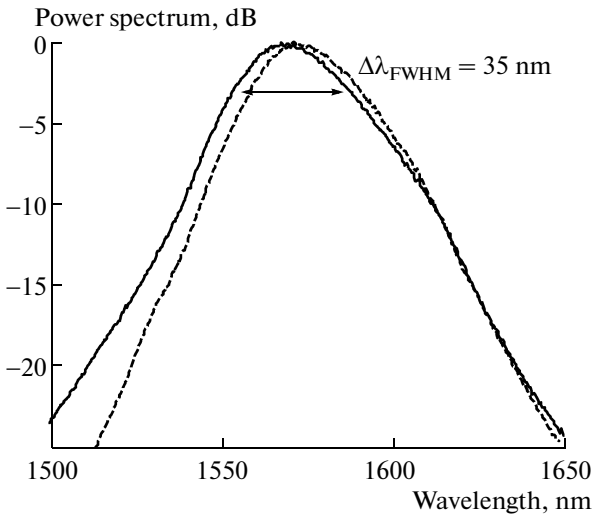

Fig. 3. Optical spectra of the mode locked pulses observed at Outputs 1 (solid) and 2 (dotted) for $\Delta\lambda_{FWHM} = 35$ nm.

$$\beta = \frac{2}{3}\gamma. \quad (2)$$

On the other hand, the QWR angle α allows precise adjustment of the NOLM low-power transmission, which is a key parameter for mode locking operation, and to allow self starting [14]. Let us assume for example that the QWR angle is adjusted for zero low-power transmission. Then, for linear input polarization forming an angle ψ with respect to the QWR axes, the NOLM transmission writes as

$$T = 0.5 - 0.5\cos\left(\frac{\pi P_{in}}{P_{\pi\psi}}\right), \quad (3)$$

where P_{in} is the NOLM input power and $P_{\pi\psi}$ is the switching power [Eq. (1)], which can be adjusted between $P_\pi = 4\pi/\beta L$ and infinity by adjusting the angle ψ. For the parameters of this experiment, we find that the minimum switching power $P_\pi \approx 125$ W. This mode of operation of the NOLM under linear input polarization was previously demonstrated theoretically [25] and experimentally [26]. Although these results are valid strictly speaking in the continuous-wave approximation only (case of large, ns pulses), they still apply qualitatively when ultrashort pulses are considered, at least if they are relatively close to fundamental solitons [27]. Finally, it should be mentioned that the same behavior is obtained when the QWR angle is adjusted for nonzero low-power transmission of the NOLM, as it usually happens in a figure-eight laser (because the onset of lasing requires some leakage through the NOLM at low power).

For the ring cavity we use a 4-m long Erbium-doped fiber (EDF), with 1000 ppm erbium concentration. The EDF was pumped by a 980 nm laser diode through a WDM coupler. We estimate that the maximum pump power that can be coupled into the fiber is around 300 mW. A polarizer is inserted in the ring to ensure linear input polarization to the NOLM, as well as a polarization controller (PC) consisting of two retarder plates, which is used to maximize the power transmission through the polarizer. The unidirectional laser operation is ensured by an optical isolator inserted in the ring cavity. The 90/10 couplers provide the. laser output ports (Outputs 1 and 2 in Fig. 1). A half wave retarder (HWR) plate controls the angle of linear polarization at the NOLM input.

2. EXPERIMENTAL RESULTS

The experimental measurements show that for different positions of the plates, continuous-wave operation is observed near 1550 nm. In our experiment self-starting mode locking operation was not observed. However, for some positions of the wave retarders, a mechanical stimulation results in a sudden widening of the spectrum to a bandwidth of several tens of nanometers, which indicates the onset of mode locking. The optical signal detected with a 2-GHz photodetector and measured on a 500-MHz oscilloscope shows a periodic pulse train with a repetition rate of 1.6-MHz, indicating fundamental frequency mode locking of the 120-m long laser cavity (Fig. 2).

The highest output power is observed at Output 1, where it reaches up to ~4 mW (this value depending on the adjustment of the wave retarders, in particular the PC). However, regardless of their power both outputs of the laser exhibited a similar behavior. Figure 3 shows the optical spectrum for the two outputs of the figure-eight laser scheme. In this case: is appreciated the output spectrum for a specific adjustment of the wave retarders, corresponding to a value of full width at half maximum (FWHM) bandwidth $\Delta\lambda_{FWHM}$ equal to 35 nm. The spectrum at Output 2 is similar to the,

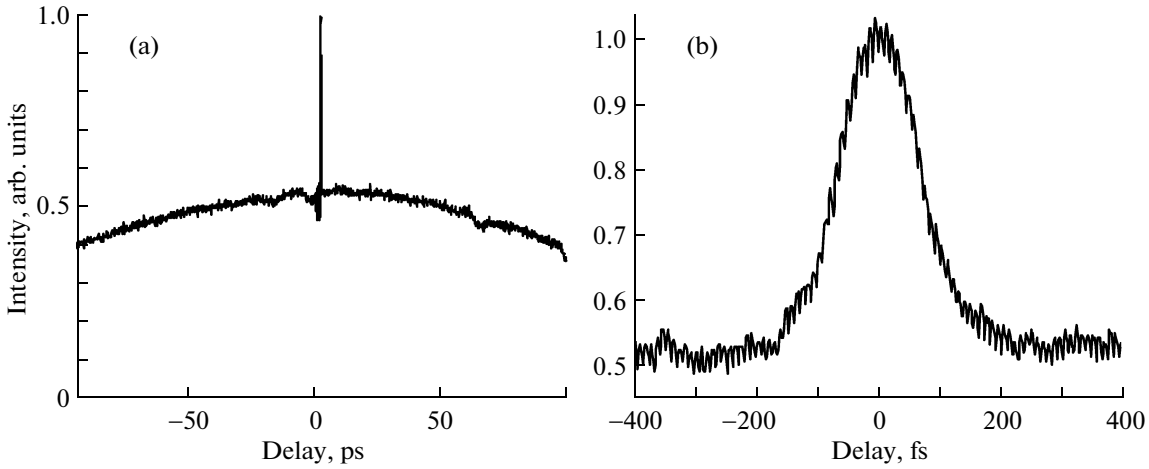

Fig. 4. Autocorrelation traces measured with two different time scales for $\Delta\lambda_{FWHM} = 35$ nm.

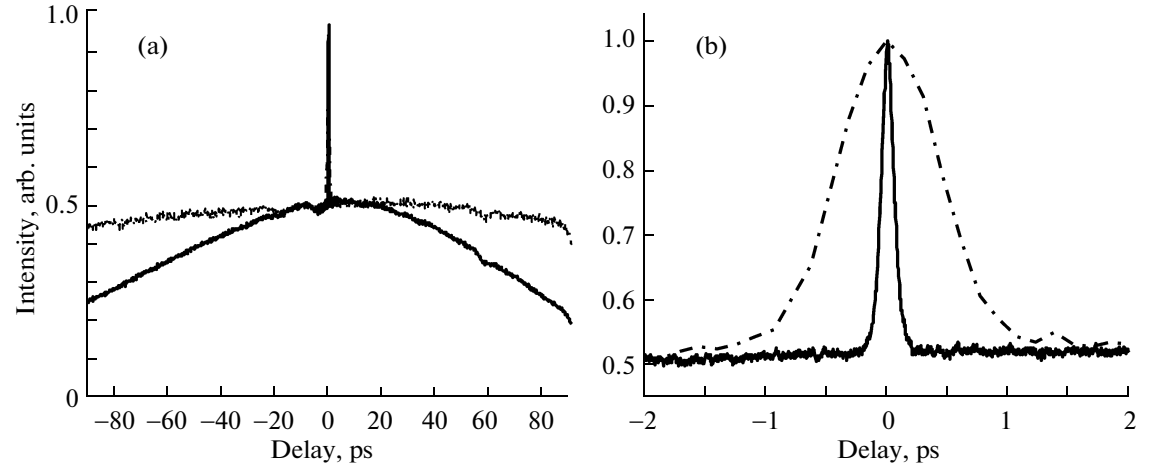

Fig. 5. Autocorrelation traces measured directly at laser output and after 760 m of SMF-28 fiber.

one measured at Output 1, except for a slight red shift which is attributed to Raman self-frequency shift occurring in the NOLM. If the HWR angle is varied around this position, we observe that the signal bandwidth can be adjusted between 16 and 52 nm, before mode locking is lost. This dependence is related to the variation of the NOLM switching power as the polarization angle at the NOLM input varies.

Figure 4 shows the autocorrelation of the optical spectrum for $\Delta\lambda_{FWHM} = 35$ nm. The trace shows a narrow sub-ps peak riding a wide pedestal that extends beyond the 200 ps measurement window. For this case, the ratio between narrow peak and pedestal level is 2 : 1. Moreover, in all cases studied, the ratio between the peak intensity and the pedestal level is ~2.

In order to assess the temporal coherence of the pulses, we measured their autocorrelation after propagation through a long dispersive medium. In this case, the spectral bandwidth was ΔFWHM = 52 nm. Figure 5 presents the autocorrelation traces directly at the laser output and after 760 m of SMF-28 fiber (D = 17 ps/nm/km). We see that, after propagation through the fiber, the central peak is still observed at the fiber output, even if it is substantially broadened (8 times) and the autocorrelation intensity is reduced. In comparison, a trans form-limited sub-ps pulse with comparable bandwidth would vanish completely over such a length due to fiber dispersion. By using a tunable attenuator at the fiber input, we verified that the shape and duration of the autocorrelation is independent of input pulse power, which shows that the soliton effect has no relevant role in preventing the pulse from vanishing. With the results obtained we can determine that the coherence of pulses is small, which is a desirable characteristic for some applications, for example in metrology [19].

The energy of pulses at Output 1 (the highest-power output of the laser) was experimentally measured, obtaining a value of ~1.4 nJ. The results of this

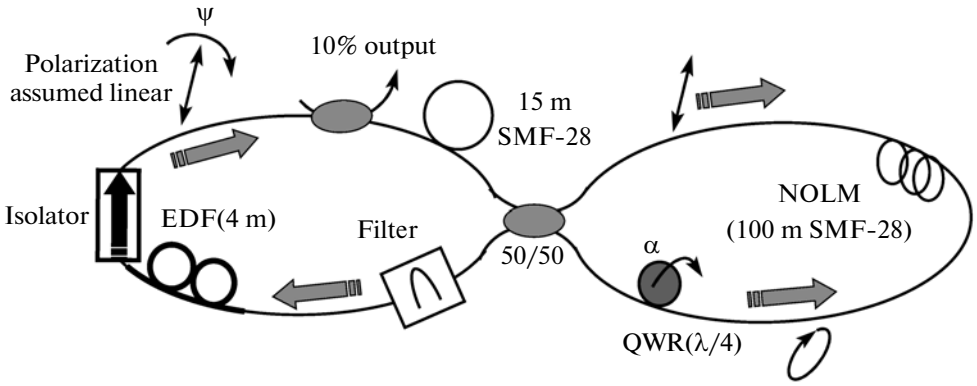

Fig. 6. Scheme of the figure-eight laser used for numerical simulations.

section show that the pulses exhibit features such as: a smooth spectral width, a wide temporal extension and small temporal coherence. From these properties we suspect that the pulses obtained are actually bunches of solitons. In the following section, we carry out a numerical study in order to assess this assumption.

3. NUMERICAL STUDY AND DISCUSSION

The figure-eight laser operation was analyzed through numerical simulations. The scheme used for this numerical analysis, which is shows in Fig. 6, is very similar to the experimental setup (Fig. 1). The length of the NOLM (100-m) and of the EDF (4-m) are chosen equal to the experiment, and a piece of 15-m of fiber is considered at the NOLM input to account for the pigtails of the components inserted in the ring section of Fig. 1 (couplers, isolator, polarizer and wave plates). Moreover, the values chosen for fiber dispersion (17 ps (nm km)$^{-1}$ and nonlinear coefficient γ (1.5 (W km)$^{-1}$) are those of the SMF-28 fiber used in the experiment. The QWR angle is set to a value ensuring low-power NOLM transmission ≈0.1, and the polarization at the NOLM input, which is assumed to be linear, makes an angle $\psi = 0.35\pi/4$ with respect to the QWR, yielding a switching power ≈240 W [see Eq. (1)], substantially higher than the minimal value of ~125 W obtained for $\psi = \pi/4$. Propagation in the fiber sections of the laser is modeled using a pair of extended nonlinear Schrödinger equations, which are integrated using the Split-Step Fourier method. In the circular polarization basis [C^+, C^-], these equations write as [28]

$$\begin{aligned}\frac{\partial C^+}{\partial z} &= -j\frac{\beta_2}{2}\frac{\partial^2 C^+}{\partial t^2} + j\beta\left(\left|C^+\right|^2 + 2\left|C^-\right|^2\right)C^+ + \frac{g}{2}C^+;\\ \frac{\partial C^-}{\partial z} &= -j\frac{\beta_2}{2}\frac{\partial^2 C^-}{\partial t^2} + j\beta\left(\left|C^-\right|^2 + 2\left|C^+\right|^2\right)C^- + \frac{g}{2}C^-.\end{aligned} \quad (4)$$

The first two right-hand terms of Eq. (4) are dispersive and Kerr nonlinear terms. The third terms are gain terms, which are considered only for integration over the gain section. The coefficient β_2 is the dispersion (expressed in ps^2/km), and g is the gain per unit length. Here, g is assumed to be constant along the doped fiber, and saturates on the pulse energy E_p as

$$g(E_p) = \frac{g_0}{1 + E_p/E_{\text{sat}}}, \quad (5)$$

where g_0 is the small-signal gain and E_{sat} is the saturation energy. The value of g_0 was chosen large enough to ensure that low-power gain exceeds the low-power cavity losses and the value of E_{sat} (0.8 nJ) was chosen in order to obtain results comparable with the experiment, in particular in terms of pulse energy. The spectral dependence of gain is taken into account through the inclusion of a Gaussian filter at the NOLM output with 1550 nm central wavelength and 50 nm FWHM bandwidth. Finally, the twist-induced group-velocity mismatch between circular polarization components in the NOLM, as well as higher-order effects like the Raman self-frequency shift and third-order dispersion were not accounted for in the model, as we believe that they are not essential to pulse formation and would not alter drastically the numerical results.

The integration begins by taking a small-amplitude Gaussian noise as the initial signal. This signal is then propagated over several cycles, and we observe whether a steady-state can be reached or not after a finite number of integration cycles. With the parameters of this study, a strict-sense convergence was not observed, however after a sufficient number of integration cycles (typically 20–25) a globally stable output waveform is obtained. Although the detailed shape of the waveform changes after successive round-trips, its general features, in particular its total duration, peak power and optical bandwidth remain stable (Figs. 7a, 7b). The waveform corresponds to a sub-ns packet containing a large number of sub-ps solitons with variable intensities. This convergence (in the broad sense) is maintained over a reasonable range of the laser parameters. For the parameters detailed previously,

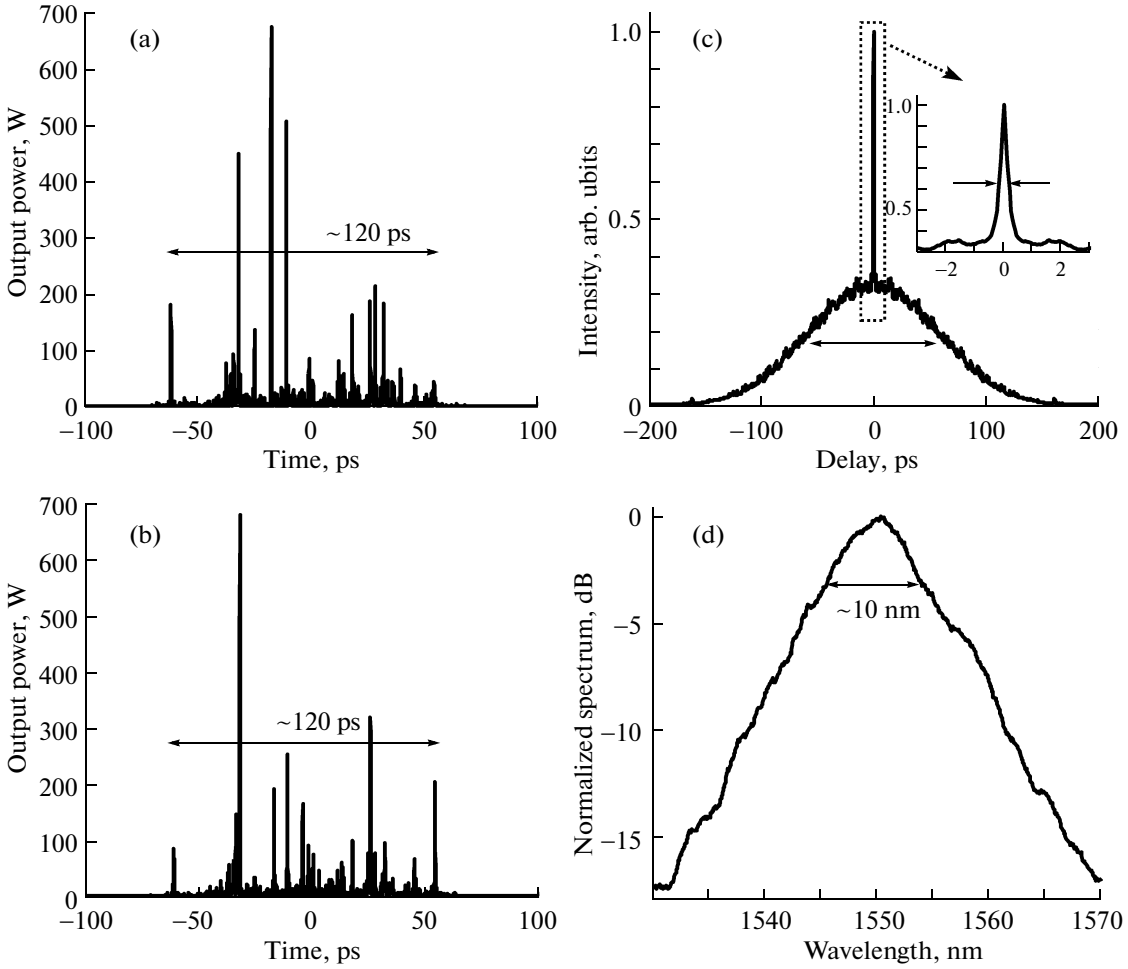

Fig. 7. Results of the numerical study; (a, b) waveforms at Output 1 for two nonconsecutive iterations; (c) autocorrelation trace, and (d) optical spectrum averaged over 10 consecutive iterations.

the total duration of the packet is ~120 ps, whereas the individual solitons in the set have different durations (depending on their peak power), scaling on average as ~100 fs. The energy of the waveform is 1.4 nJ, like in the experiment.

Figure 7c presents the simulated autocorrelation trace averaged over 10 pulses. Its general shape is in accordance with the experimental results of Fig. 4, with a sub-fs central peak riding a sub-ps pedestal. The extension of the pedestal reflects the total duration of the waveform, whereas that of the narrow central peak reflects the duration of the solitons in the set. One difference with the experiment however is that the ratio between the central peak power and pedestal level in the simulated autocorrelation is higher than 2, and generally varies with the simulation parameters. Finally, Fig. 7d shows the optical spectrum averaged over 10 pulses. A relatively wide and smooth spectrum is obtained, which is consistent with the experimental results (Fig. 3), although the FWHM bandwidth is not larger than 10 nm in the numerical study.

The process of pulse formation in this laser, under the combined action of anomalous dispersion and Kerr nonlinearity [see Eq. (4)] is intimately related to the modulation instability mechanism, through which a quasi-continuous-wave beam, in the presence of noise, transforms into a packet of a large number of solitons with widely distributed amplitudes [29]. The NOLM also plays an important role in pulse formation. In particular, Figs. 7a, 7b shows that many pulses in the set arrive at the NOLM input with a power that is many times the NOLM switching power. As a consequence, they tend to split into multiple pulses at the NOLM output. The NOLM thus tends to increase the number of pulses in the set. Moreover, the NOLM is also essential as it stabilizes the pulse duration, eliminating the low-power skirts of the waveform which tends to broaden through propagation in the dispersive fiber.

4. CONCLUSIONS

In conclusion, we studied the generation of long broadband pulses through a figure-eight laser scheme,

which includes a polarization-imbalanced NOLM with linear polarization at the input. For some adjustments of the wave retarders and under mechanical stimulation, a stable train of sub-nanosecond pulses at 1.6-MHz repetition rate is generated by the laser, indicating fundamental frequency mode locking of the 120-m long laser cavity. An output pulse energy as high as 1.4 nJ was obtained experimentally without any dispersion management. The measured pulse characteristics include a large duration in the order of hundreds of ps, a short temporal coherence in the order of 100 fs and a very large spectral bandwidth (several tens of nanometers). The experimental results suggest that the pulses are actually bunches of solitons, whose durations are of the order of ~100 fs. This assumption was confirmed through numerical simulations of the proposed laser scheme, which showed that modulational instability and NOLM overdriving play an essential part in the mechanism of pulse formation. The pulses from the figure-eight laser operated in this regime present relatively high energy and low coherence, these features may be attractive for applications in metrology and for seeding supercontinuum generation.

ACKNOWLEDGMENTS

This work was funded by CONACyT project no. 53990. J.C. Hernandez-Garcia was suported by CONACyT grant no. 217385.

REFERENCES

1. Z. C. Luo, A. P. Luo, W. C. Xu, C. X. Song, Y. X. Gao, and W. C. Chen, Laser Phys. Lett. **6**, 582 (2009).
2. Z. X. Zhang, L. Zhan, X. X. Yang, S. Y. Luo, and Y. X. Xia, Laser Phys. Lett. **4**, 592 (2007).
3. L. R. Wang, X. M. Liu, and Y. K. Gong, Laser Phys. Lett. **7**, 63 (2010).
4. H. Zhang, D. Y. Tang, L. M. Zhao, Q. L. Bao, K. P. Loh, B. Lin, and S. C. Tjin, Laser Phys. Lett. **7**, 591 (2010).
5. D. Mao, X. M. Liu, L. R. Wang, X. H. Li, H. Lu, H. B. Sun, and Y. K. Gong, Laser Phys. **20**, 847 (2010).
6. I. N. Duling III, Opt. Lett. **16**, 539 (1991).
7. Z. X. Zhang, Z. Q. Ye, M. H. Sang, and Y. Y. Nie, Laser Phys. Lett. **5**, 364 (2008).
8. N. J. Doran and D. Wood, Opt. Lett. **13**, 56 (1998).
9. M. E. Fermann, F. Haberl, and M. Hofer, Opt. Lett. **15**, 752 (1990).
10. Y. H. Zhong, Z. X. Zhang, and X. Y. Tao, Laser Phys. **20**, 1756 (2010).
11. M. Zhang, L. L. Chen, C. Zhou, Y. Cai, L. Ren, and Z. G. Zhang, Laser Phys. Lett. **6**, 657 (2009).
12. E. A. Kuzin, N. Korneev, J. W. Haus, and B. Ibarra-Escamilla, J. Opt. Soc. Am. B **18**, 919 (2001).
13. E. A. Kuzin, B. Ibarra-Escamilla, D. E. Garcia-Gomez, and J. W. Haus, Opt. Lett. **15**, 1559 (2001).
14. B. Ibarra-Escamilla, O. Pottiez, E. A. Kuzin, J. W. Haus, R. Grajales-Coutiño, and P. Zaca-Moran, Opt. Commun. **281**, 1226 (2008).
15. O. Pottiez, R. Grajales-Coutiño, B. Ibarra-Escamilla, E. A. Kuzin, J. C. Hernandez-Garcia, and A. Gonzalez-Garcia, in *Proceedings of SPIE Photonics Europe 2010, Brussels, Belgium, 12–16 April 2010*, Proc. SPIE 7721, 77210A (2010).
16. K. Mori, H. Takara, and S. Kawanichi, J. Opt. Soc. Am. B. **18**, 1780 (2001).
17. S. O. Konorov, E. E. Serebryannikov, Ping Zhou, A. V. Khokhlov, V. S. Shevandin, K. V. Dukel'skii, Yu. N. Kondrat'ev, D. A. Sidorov-Biryukov, A. B. Fedotov, A. P. Tarasevitch, D. von der Linde, and A. M. Zheltikov, Laser Phys. Lett. **1**, 199 (2004).
18. Z. X. Zhang, K. Xu, J. Wu, X. B. Hong, and J. T. Lin, Laser Phys. Lett. **5**, 213 (2008).
19. M. Horowitz, Y. Barad, and Y. Silberberg, Opt. Lett. **22**, 799 (1997).
20. I. N. Duling III, Electron. Lett. **27**, 544 (1991).
21. K. Tamura, E. P. Ippen, H. A. Haus, and L. E. Nelson, Opt. Lett. **18**, 1080 (1993).
22. L. E. Nelson, S. B. Fleischer, G. Lenz, and E. P. Ippen, Opt. Lett. **21**, 1759 (1996).
23. B. W. Liu, M. L. Hu, X. H. Fang, Y. Z. Wu, Y. J. Song, L. Chai, C. Y. Wang, and A. M. Zheltikov, Laser Phys. Lett. **6**, 44 (2009).
24. T. Tanemura and K. Kikuchi, J. Lightwave Technol. **24**, 4108 (2006).
25. O. Pottiez, E. A. Kuzin, B. Ibarra-Escamilla, and F. Mendez-Martinez, Opt. Commun. **254**, 152 (2005).
26. B. Ibarra-Escamilla, E. A. Kuzin, P. Zaca-Moran, R. Grajales-Coutiño, F. Mendez-Martinez, O. Pottiez, R. Rojas-Laguna, and J. W. Haus, Opt. Express **13**, 10760 (2005).
27. O. Pottiez, B. Ibarra-Escamilla, and E. A. Kuzin, Opt. Fiber Technol. **15**, 172 (2009).
28. G. P. Agrawal, *Nonlinear Fiber Optics* (Academic, San Diego, 1995).
29. V. E. Zacharov and A. B. Shabat, Sov. Phys. JETP **61**, 62 (1972).